

# Application of a transition metal oxide/carbon-based nanocomposite for designing a molecularly imprinted poly (L-cysteine) electrochemical sensor for curcumin

Arash Mohammadinejad<sup>a,b,g</sup>, Ebrahim Abouzari-Lotf<sup>c,d</sup>, Ghazaleh Aleyghoob<sup>g</sup>,  
Majid Rezayi<sup>e,f,g,\*</sup>, Reza Kazemi Oskuee<sup>b,g,\*</sup>

<sup>a</sup> Targeted Drug Delivery Research Center, Institute of Pharmaceutical Technology, Mashhad University of Medical Sciences, Mashhad, Iran

<sup>b</sup> Applied Biomedical Research Center, Mashhad University of Medical Sciences, Mashhad, Iran

<sup>c</sup> Electrochemical Energy Storage, Helmholtz Institute Ulm (HIU), Helmholtzstraße 11, Ulm, D-89081 Germany

<sup>d</sup> Institute of Nanotechnology, Karlsruhe Institute of Technology, P.O. Box 3640, 76021 Karlsruhe, Germany

<sup>e</sup> Medical Toxicology Research Center, Mashhad University of Medical Sciences, Mashhad, Iran

<sup>f</sup> Metabolic Syndrome Research Center, School of Medicine, Mashhad University of Medical Sciences, Mashhad, Iran

<sup>g</sup> Department of Medical Biotechnology and Nanotechnology, School of Medicine, Mashhad University of Medical Sciences, Mashhad, Iran

## ARTICLE INFO

### Keywords:

Curcumin  
Transition metal oxide  
Carbon nanotubes  
Graphene oxide  
L-cysteine  
Molecularly imprinted polymer

## ABSTRACT

In this study an electrochemical sensor was fabricated for detection of curcumin, as a functional herbal food, using molecularly imprinted polymer and highly conductive transition metal oxide/carbon-based nanocomposite. In this way, CuCo<sub>2</sub>O<sub>4</sub>/nitrogen-doped carbon nanotubes/phosphorus-doped graphene oxide nanocomposite was dropped on the electrode. This nanocomposite synergically possesses conductivity features of copper and phosphorus-doping sites, specific surface area of carbon nanotubes, and carbons Fermi level of graphene oxide. In the following, L-Cystein electropolymerized on the electrode in presence of curcumin. The sensor was produced by removing curcumin from poly (L- cystein) matrix. The sensor was successfully used for detection of curcumin in the ranges of 0.1–1 μmol L<sup>-1</sup> and 1–30 μmol L<sup>-1</sup>, with acceptable detection limit (30 nmol L<sup>-1</sup>). Finally, the proposed method was used for detection of curcumin in serum samples with recoveries of 80–110.87%. The results demonstrated that aforementioned method can be used for detection of curcumin in biological samples.

## 1. Introduction

Curcumin (CUR), as a diketone, 1,7-bis-(4-hydroxy-3-methoxyphenyl)-1,6-heptadiene- 2,5-dione, can be extracted from turmeric rhizome which belongs to the ginger family. CUR has been widely used with dietary and therapeutic aims. This compound, as natural pigment with bright yellow color, can be applied in industrial dyeing consumptions such as production of cakes, canned foods, and beverages. Also due to functional effects of anti-oxidizing, anti-bacterial, anti- carcinogenicity, anti-inflammatory, and anti-HIV, this compound is considered as a potent herbal agent in biology and pharmacology (Neerati, Devde, & Gangi, 2014). So, because of growing use of CUR as a functional herbal

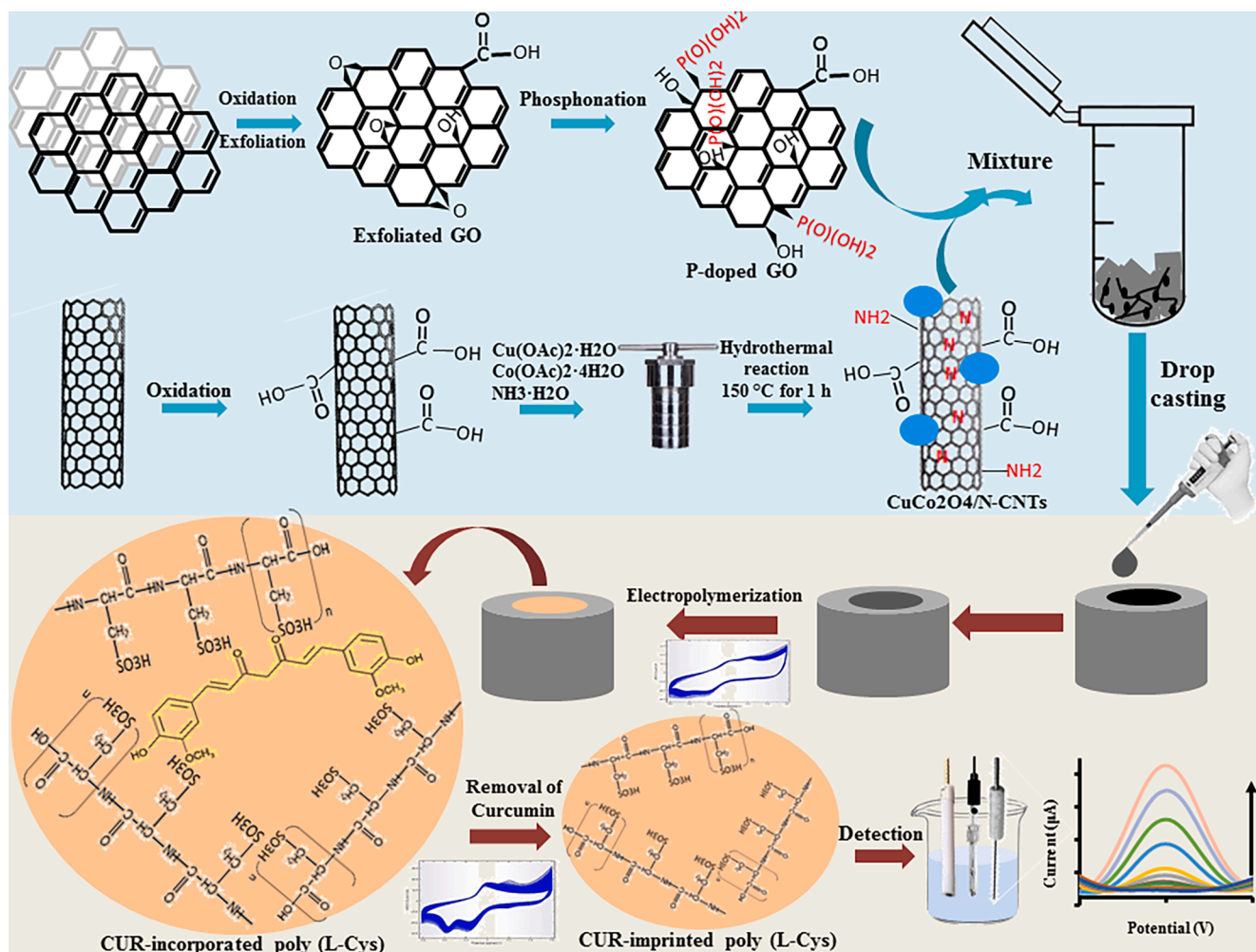
food, the development of the analytical method for its quantification in biological and food samples is highly demanded.

Up to now several analytical methods have been developed for detection of CUR such as liquid chromatography, capillary electrophoresis (CE), spectrophotometry, resonance light scattering (RLS) and spectrofluorimetry (Liu, Gong, Dong, Zhou, Shuang, & Dong, 2018). Although these methods may possess high enough sensitivity and accuracy, but they suffer from requirement of costly equipment and reagents, boring and complex sample preparation, lack of selectivity and expert persons. In comparison with aforementioned methods, electrochemical sensors are highly simple, sensitive and facile which can be a powerful alternative of traditional methods for CUR detection.

**Abbreviations:** CUR, Curcumin; MIP, Molecularly imprinted polymer; P-GO, Phosphorous-doped graphene oxide; N-CNTs, Nitrogen-doped carbon nanotubes; L-Cys, L-cysteine.

\* Corresponding authors at: Medical Toxicology Research Center, Mashhad University of Medical Sciences, Mashhad, Iran (M. Rezayi). Department of Medical Biotechnology and Nanotechnology, School of Medicine, Mashhad University of Medical Sciences, Mashhad, Iran (R. Kazemi Oskuee).

E-mail addresses: [Rezaeimj@mums.ac.ir](mailto:Rezaeimj@mums.ac.ir) (M. Rezayi), [oskueekr@mums.ac.ir](mailto:oskueekr@mums.ac.ir) (R. Kazemi Oskuee).



**Scheme 1.** Synthesis process of  $\text{CuCo}_2\text{O}_4/\text{N-CNTs}$  and P-GO and also preparation of L-(Cys)-based MIP sensor for CUR.

Recently modification of electrochemical sensors with metal nanoparticles, and carbon nanomaterials has gained considerable attention. Carbon nanotubes (CNTs) with significant conductivity and high surface area are a potent modifier agent for electrochemical sensors. Moreover doping of nitrogen can lead to the enhancement of conductivity, and stability of CNTs (Zhang, Sui, Xue, Wang, Pei, Liang, et al., 2019).

$\text{CuCo}_2\text{O}_4$  nanomaterials, as oxides of transition metal, possess unbelievable properties such as stability, catalytic effects, simple and low-cost synthesis, specific surface area and conductivity. So, incorporation of  $\text{CuCo}_2\text{O}_4$  nanomaterials with CNTs can devote excellent electrochemical features to sensors.

Graphene as 2D carbon material contain packed carbon atoms in unit sheet of hexagonal structure. Graphene with interesting physical, electrical and optical features, have been an attractive material for fabrication of sensors. The possible irreversible agglomeration of graphene nanosheets due to  $\pi$ - $\pi$  and Van-der-Waals interactions may limit its application. Collaboration of 1D CNTs with graphene can improve efficiency of graphene through playing role of electron transfer between sheets and prevention of agglomeration. On the other hand chemical doping of graphene by heteroatoms such as sulfur, nitrogen, phosphorus, and boron can lead to prevention of aggregation and enhancement of conductivity (Xu, Liu, Chen, Li, Tang, & Li, 2017).

Molecularly imprinted polymers (MIP) as a cross-linked polymer are commonly formed through electrochemically polymerization of functional monomers and template on the sensors. MIP contains recognition sites formed by interaction between template and monomer followed by extraction and removal of template. So, MIP can improve the specifically

recognition ability of sensors to template.

In this study glassy carbon electrode (GCE) was modified by  $\text{CuCo}_2\text{O}_4$ /nitrogen-doped CNTs/phosphorous-doped graphene oxide nanocomposite ( $\text{CuCo}_2\text{O}_4/\text{N-CNTs}/\text{P-GO}$ ) followed by electropolymerization of L-cysteine (L-Cys), as functional monomer, in presence of CUR (Scheme 1). L-Cys as an important amino acid is able to be applied for electropolymerization due to the electro activity of amino and thiol groups. Based on our knowledge the application of  $\text{CuCo}_2\text{O}_4/\text{N-CNTs}/\text{P-GO}$  nanocomposite and incorporation of  $\text{CuCo}_2\text{O}_4/\text{N-CNTs}/\text{P-GO}$  with MIP for the first time have been performed for designing a sensor for CUR detection. Finally, the designed electrode was successfully used for detection of CUR in serum sample.

## 2. Material and methods

### 2.1. Chemicals

Copper (II) acetate monohydrate ( $\text{Cu}(\text{OAc})_2 \cdot \text{H}_2\text{O}$ ), Cobalt (II) acetate tetrahydrate ( $\text{Co}(\text{OAc})_2 \cdot 4\text{H}_2\text{O}$ ), CUR, potassium ferricyanide ( $\text{K}_3[\text{Fe}(\text{CN})_6]$ ), monobasic sodium phosphate ( $\text{NaH}_2\text{PO}_4$ ), dibasic sodium phosphate ( $\text{Na}_2\text{HPO}_4$ ), phosphoric acid (85%, analytical grade), graphite flakes (grade 230U, 325 mesh), polyphosphoric acid (105%  $\text{H}_3\text{PO}_4$  basis), multi-walled carbon nanotubes (MWCNTs), L-Cys, potassium permanganate ( $\text{KMnO}_4$ ), potassium nitrate ( $\text{KNO}_3$ ), were all obtained from Sigma-Aldrich (USA). All solvents with analytical grade such as ethanol, sulphuric acid ( $\text{H}_2\text{SO}_4$ ), hydrochloric acid (HCl), ammonia solution ( $\text{NH}_3 \cdot \text{H}_2\text{O}$ ) and hydrogen peroxide ( $\text{H}_2\text{O}_2$ ) were

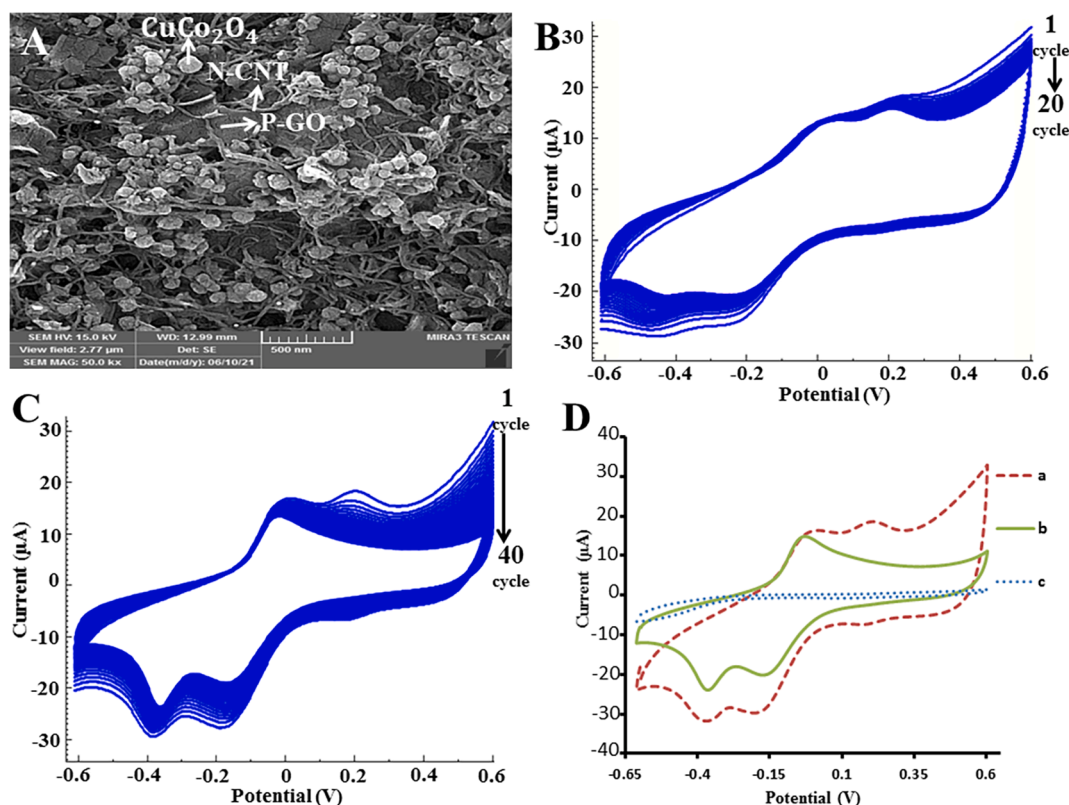


**Fig. 1.** (A) Surface morphology evaluation of  $\text{CuCo}_2\text{O}_4/\text{N-CNTs}/\text{P-GO}$  nanocomposite using FESEM; (B) electropolymerization of  $\text{l-Cys}$  on  $\text{GCE}/\text{CuCo}_2\text{O}_4/\text{N-CNTs}/\text{P-GO}$  surface by CV (20 cycles); (C) Removal of CUR from  $\text{GCE}/\text{CuCo}_2\text{O}_4/\text{N-CNTs}/\text{P-GO}/\text{CUR}$ - incorporated poly ( $\text{l-Cys}$ ) by CV (40 cycles); (D) comparison of cyclic voltammograms of: (a)  $\text{GCE}/\text{CuCo}_2\text{O}_4/\text{N-CNTs}/\text{P-GO}/\text{CUR}$ -incorporated poly( $\text{l-Cys}$ ), (b),  $\text{GCE}/\text{CuCo}_2\text{O}_4/\text{N-CNTs}/\text{P-GO}/\text{CUR}$ -imprinted poly ( $\text{l-Cys}$ ), and (c) GCE in scan rate of  $50 \text{ mVs}^{-1}$  and in pH 7 PBS ( $0.05 \text{ mol L}^{-1}$ ). Condition: Start and stop potential:  $-0.6$ , Upper potential:  $0.6$ , Number of cycles: 20 cycles (for electropolymerization), and 40 cycles (for CUR removal), Electrolyte of polymerization and CUR removal: PH 7 PBS ( $0.05 \text{ mol L}^{-1}$ ), CUR to  $\text{l-Cys}$  mole ratio: 1:2.

purchased from Merck (USA). The stock solution of CUR was prepared by ethanol and was kept in dark and  $4^\circ\text{C}$  until use.

## 2.2. Instruments

All electrochemical detection processes were performed using Autolab potentiostat–galvanostat three-electrode system (PGSTAT204, Metrohm, Herisau, Switzerland) containing  $\text{Ag}/\text{AgCl}$  reference electrode, platinum counter electrode and GCE as working electrode. The studies of electrochemical impedance spectroscopy (EIS) were performed by Autolab 302 N system. Analysis of data was done by NOVA 1.11 software. A LEO 912AB (120 kv, Germany) system was used to obtain transmission electron microscopy (TEM) image. X-ray spectroscopy (EDX) image, surface morphology and elemental MAPING were obtained by a MIRA3 TESCAN (USA) Field Emission Scanning Electron Microscope (FE-SEM) with LVSTD detector (USA). Energy-dispersive X-ray diffraction (XRD) spectra was recorded by an Explorer system (GNR Co., Italy) equipped with a radiation source of  $\text{Cu K}\alpha$  ( $1.54187 \text{ \AA}$ ) and Scintillator detector working at conditions of 30 mA, 40 kV and room temperature. A NanoWizard II system (JPKCo., Germany) was used for preparing atomic force microscopy (AFM) images. Fourier transform infrared (FTIR) spectra were achieved by Thermo Nicolet spectrophotometer (made in USA, model of AVATAR 370). The studies of X-ray photoelectron spectroscopy (XPS) for obtaining the binding energies of nanoparticles were done by PHI Quantera II Scanning XPS Microprobe equipped with a  $\text{Al K}\alpha$  anode as monochromatic radiation source under conditions of  $1486.6 \text{ eV}$ , pressure  $< 2 \times 10^{-6}$  bar and room temperature.

## 2.3. Synthesis of $\text{CuCo}_2\text{O}_4/\text{N-CNTs}$

Preparation of  $\text{CuCo}_2\text{O}_4/\text{N-CNTs}$  was done according to the previous studies with some modifications (P. Liang, Wang, & Hu, 2018). Firstly, for oxidation, 100 mg MWCNTs were added to 23 mL sulfuric acid followed by stirring for 12 h. After sequentially addition of 416 mg  $\text{KNO}_3$  and 1 g  $\text{KMnO}_4$  to the mixture in a  $40^\circ\text{C}$  water bath, 6 mL water was sectionally added with an interval time of 5 min. Then after another 5 min, 15 mL water was added and the mixture stayed unchanged for 15 min. Afterwards 10 mL  $\text{H}_2\text{O}_2$  (30%) and 140 mL water were added to complete the oxidation reaction. The resultant was collected and washed with water and HCl (5%) solution. Afterwards, 0.086 g of oxidized CNTs sonicated in 4 mL of water–ethanol composition (4:96, v/v %). After addition of 0.128 g  $\text{Cu}(\text{OAc})_2 \cdot \text{H}_2\text{O}$  and 0.31 g  $\text{Co}(\text{OAc})_2 \cdot 4\text{H}_2\text{O}$ , 0.5 mL  $\text{NH}_3 \cdot \text{H}_2\text{O}$  was added and mixture was stirred for 24 h at  $80^\circ\text{C}$ . After addition of aforementioned mixture to the stainless-steel autoclave reactor, hydrothermal reaction was processed at  $150^\circ\text{C}$  for 1 h. After completion of reaction, the resultant was centrifuged, collected, washed with ethanol–water (50:50, v/v %) and freeze-dried.

## 2.4. Synthesis of P-GO

The protocol of synthesis was processed with orderly performance of three steps containing oxidation, exfoliation and phosphonation according to the previous reported studies (Abouzari-Lotf, Zakeri, Nasef, Miyake, Mozarmnia, Baziliah, et al., 2019). Firstly, GO was obtained by oxidation of graphite flakes according to the Hummers and Offeman method followed by exfoliation step which was performed by ultrasonication of resultant ( $4 \text{ mg mL}^{-1}$ ) in water. In order to removal of unexfoliated residual, the mixture was centrifuged for 15 min ( $1610 \text{ g}$ ,

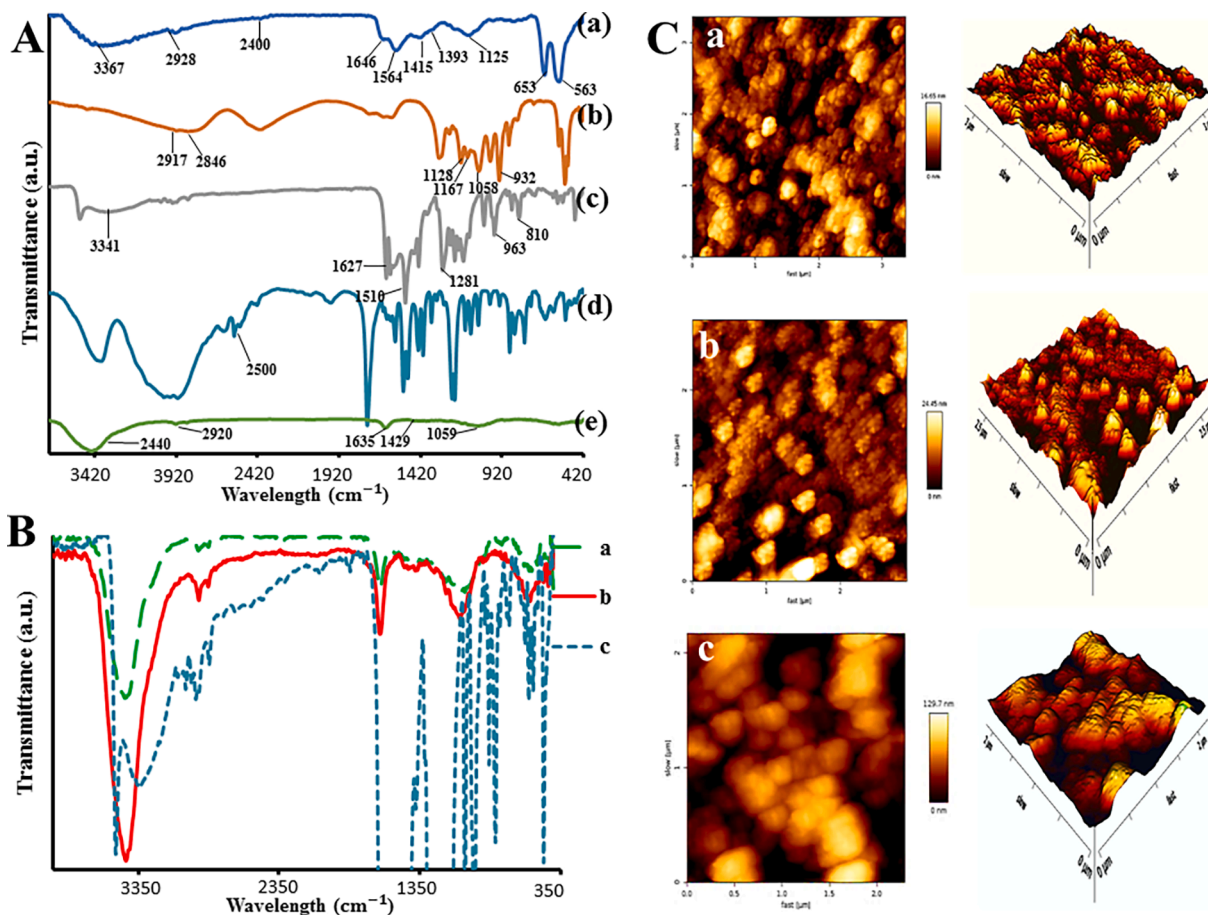


**Fig. 2.** Characterization of sensor: (A) (a-e) FT-IR spectra of: (a)  $\text{CuCo}_2\text{O}_4/\text{N-CNTs}$ , (b) P-GO, (c) CUR, (d) L-Cys, (e)  $\text{CuCo}_2\text{O}_4/\text{N-CNTs}/\text{P-GO}/\text{CUR}$ -imprinted poly (L-Cys); (B) (a-c) FT-IR spectra of: (a)  $\text{CuCo}_2\text{O}_4/\text{N-CNTs}/\text{P-GO}/\text{CUR}$ -imprinted poly (L-Cys), (b)  $\text{CuCo}_2\text{O}_4/\text{N-CNTs}/\text{P-GO}/\text{CUR}$ -incorporated poly (L-Cys), (c) CUR; (C) (a-c) AFM topographies of (a) GCE/  $\text{CuCo}_2\text{O}_4/\text{N-CNTs}/\text{P-GO}$ , (b) GCE/  $\text{CuCo}_2\text{O}_4/\text{N-CNTs}/\text{P-GO}/\text{CUR}$ -incorporated poly (L-Cys), (c) GCE/ $\text{CuCo}_2\text{O}_4/\text{N-CNTs}/\text{P-GO}/\text{CUR}$ -imprinted poly (L-Cys). Condition: Condition: Start and stop potential:  $-0.6$ , Upper potential:  $0.6$ , Scan rate:  $50 \text{ mVs}^{-1}$ , Number of cycles: 20 (for electropolymerization), 40 (for CUR removal), Electrolyte of polymerization: PH 7 PBS ( $0.05 \text{ mol L}^{-1}$ ), CUR to L-Cys mole ratio: 1:2.

$10^\circ\text{C}$ ). Finally resulted GO powder was dried in a vacuum oven at  $70^\circ\text{C}$  for 24 h. For phosphonation process a mixture of polyphosphoric acid and phosphoric acid (1:5 wt%) homogenized by sonication and its pH was adjusted to 5 and then added in to a flask. After dispersion of GO in 50 mL deionized water (DI) (0.5 wt%), the mixture was poured into the experimental flask followed by string and heating ( $95^\circ\text{C}$ ) for 8 h. Finally, the resultant centrifuged ( $12175 \text{ g}$ ,  $2^\circ\text{C}$ ), washed by DI and dried in the vacuum condition.

#### 2.5. Preparation of GCE/ $\text{CuCo}_2\text{O}_4/\text{N-CNTs}/\text{P-GO}/\text{CUR}$ -imprinted poly (L-Cys)

Firstly, for cleaning of the electrode surface, GCE was polished by alumina powder and the sonicated in water-ethanol solution (50:50, v/v %). Then, 0.7 mg  $\text{CuCo}_2\text{O}_4/\text{N-CNTs}$  and 1 mg P-GO were well dispersed in 2 mL water-ethanol (50:50, v/v %) followed by drop-casting of nano-composition on the GCE surface. In the following, the electrode was immersed in PBS ( $0.05 \text{ M}$ , pH 7) containing CUR and L-Cys with mole ratio of 1:2 and electropolymerization was done by cyclic voltammetry (CV) (20 cycles) in the potential range of  $-0.6$ – $0.6 \text{ V}$  with scan rate of  $50 \text{ mVs}^{-1}$ . For removal of CUR from poly (L-Cys) matrix, CV (40 cycles) was performed in pH 7 PBS ( $0.05 \text{ mol L}^{-1}$ ) in the potential range of  $-0.6$ – $0.6 \text{ V}$ . In order to the assessment of the stepwise modification of GCE, CV was done in  $100 \text{ mmol L}^{-1}$  KCl solution containing  $1 \text{ mmol L}^{-1}$   $\text{K}_3\text{Fe}(\text{CN})_6$ .

#### 2.6. Pretreatment of human serum samples

The blood serum sample was obtained from a local clinical pathology laboratory and used without pretreatment. According to the previous study, the serum sample was prepared by 100 times dilution (Kalam-bate, Rawool, & Srivastava, 2016) by PBS (pH 3.06,  $0.1 \text{ mol L}^{-1}$ ).

#### 2.7. Electrochemical detection

In order to the detection of CUR, in a volumetric flask a proper volume of CUR stock solution diluted by PBS (pH 3.06,  $0.1 \text{ mol L}^{-1}$ ) to 4 mL to obtain considered concentration followed by detection by differential pulse voltammetry (DPV) mode. Also, for application of detection method in real sample, prepared serum was spiked by proper volume of CUR stock solution.

### 3. Results and discussion

#### 3.1. Preparation and characterization of the sensor

In order to the characterization of sensor different microscopic, spectroscopic, and electrochemical methods were employed. Several methods of TEM, XRD, EDX and DLS were used to evaluate morphology, crystallinity, elemental analysis, size and zeta potential of  $\text{CuCo}_2\text{O}_4/\text{N-CNTs}$ . Also, characterization of P-GO was done by TEM, XRD, XPS (wide range survey and narrow scan spectra), and EDX. The explanations and

figures for individual characterization of nanoparticles were considered as [supplementary information](#). [Fig S1](#) and [Fig S2](#) presence characterization images related to  $\text{CuCo}_2\text{O}_4/\text{N-CNTs}$  and P-GO, respectively.

In order to ideal performance of electrode modification, both nanoparticles must be homogeneously mixed before dropping on the electrode surface. CUR can be adsorbed on the electrode surface through non-covalent interaction with nitrogen groups ([Mousaabadi, Ensafi, Hadadzadeh, & Rezaei, 2020](#)) and phosphonic acids groups for further polymerization process. The surface morphology of  $\text{CuCo}_2\text{O}_4/\text{N-CNTs}/\text{P-GO}$  nanocomposite was evaluated by FE-SEM technique. As presented in [Fig. 1A](#)  $\text{CuCo}_2\text{O}_4/\text{N-CNTs}$  nanoparticles and P-GO nanosheets were uniformly and homogeneously mixed and  $\text{CuCo}_2\text{O}_4/\text{N-CNTs}$  nanoparticles were well distributed among P-GO nanosheets. Moreover, incorporation of  $\text{CuCo}_2\text{O}_4$  nanoparticles with size about 100 nm on the N-CNTs was proved. In addition, elemental analysis of  $\text{CuCo}_2\text{O}_4/\text{N-CNTs}/\text{P-GO}$  nanocomposite was done by EDX and MAPING analysis ([Fig. S3](#)).

$\text{CuCo}_2\text{O}_4$  as multivalent metal oxides possess spinal structure which copper ions locate on tetrahedral position and cobalt ions locate on both tetrahedron and octahedron position (Z.-H. [Liang, Zhu, & Hu, 2004](#)). So, the L-Cys can be anchored on the surface through binding of carboxyl, thiol and amino groups of L-Cys to cobalt and copper ([Priyanga, Khamrang, Velusamy, Karthi, Ashokkumar, & Mayilmurugan, 2019; Zhou, Mo, Sun, Luo, Fan, Zhu, et al., 2022](#)). Also, hydrogen bonding of L-Cys with phosphonic acids groups of P-GO lead to anchoring on the electrode surface. Especially according to the literature, anchoring of L-Cys on the carbon groups of nanoparticles can be happened through amino groups of L-Cys during electrochemical oxidation process followed by consecutive nucleophilic acyl substitution ([He, Li, Zhang, &](#)

[Luo, 2017](#)). The incorporation of CUR in poly (L-Cys) matrix is through hydrogen bonding interactions with oxygen groups of CUR ([Scheme 1](#)).

Molecular imprinted poly (L-Cys) layer was created on the surface of GCE/ $\text{CuCo}_2\text{O}_4/\text{N-CNTs}/\text{P-GO}$  by electropolymerization of L-Cys during 20 cycles from -0.6 to 0.6 V with scan rate of  $50 \text{ mV s}^{-1}$  in pH 7 PBS ( $0.05 \text{ mol L}^{-1}$ ) containing CUR and L-Cys (CUR:L-Cys mole ratio 1:2).

As shown in the cyclic voltammograms ([Fig. 1B](#)), when cycles consecutively scanned with scan rate of  $50 \text{ mV s}^{-1}$  in the considered ranges, the oxidation and reduction peaks current of L-Cys at about 0.1 and -0.5 V were dramatically decreased which demonstrates successfully, preparation and growth of insulating polymer layer. Moreover, for removal of CUR from poly (L-Cys) and creation of specific cavities, 40 cycles were scanned ([Fig. 1C](#)) in PBS with pH 7 ( $0.05 \text{ mol L}^{-1}$ ) in the potential range of -0.6–0.6 V. According to the [Fig. 1C](#) the disappearing of anodic and cathodic peak currents at about 0.2 V during consecutive scans, obviously demonstrates the removal of CUR from poly (L-Cys) matrix. The CV results of preparation of proposed sensor are presented in [Fig. 1D](#). The increase of current of GCE/ $\text{CuCo}_2\text{O}_4/\text{N-CNTs}/\text{P-GO}/\text{CUR}$ - incorporated poly (L-Cys) ([Fig. 1D, curve a](#)) in comparison with GCE ([Fig. 1D, curve c](#)) obviously demonstrated effect of coating the electrode by  $\text{CuCo}_2\text{O}_4/\text{N-CNTs}/\text{P-GO}$  nanocomposite and poly (L-Cys). Moreover elimination of anodic and cathodic peak currents at about 0.2 V for GCE/ $\text{CuCo}_2\text{O}_4/\text{N-CNTs}/\text{P-GO}/\text{CUR}$ -imprinted poly (L-Cys) ([Fig. 1D, curve b](#)) clearly proved successfully removal CUR from poly (L-Cys) matrix.

In order to more confirmation, FT-IR spectroscopy was applied for identification of GCE modification and results are indicated in the [Fig. 2A](#). As shown in FT-IR spectrum of  $\text{CuCo}_2\text{O}_4/\text{N-CNTs}$  ([Fig. 2A, curve a](#)) the presence of -COOH groups are proven by vibration peaks

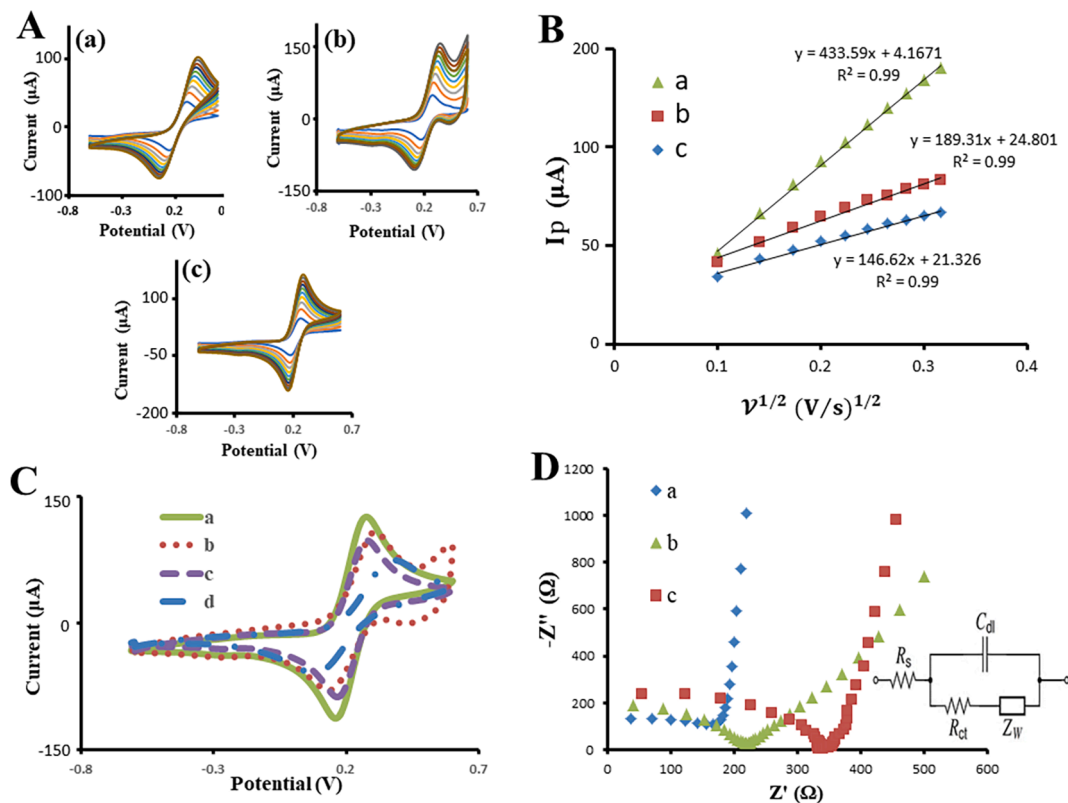


**Fig. 3.** Evaluation of surface modification by CV: (A) linear diagram of peak current of  $\text{K}_3\text{Fe}(\text{CN})_6$  ( $1 \text{ mmol L}^{-1}$ ) against square root of scan rate in the range of  $10\text{--}100 \text{ mV s}^{-1}$ ; (B) (a-c) Cyclic voltammograms of  $\text{K}_3\text{Fe}(\text{CN})_6$  ( $1 \text{ mmol L}^{-1}$ ) scanned by (a) GCE, (b) GCE/ $\text{CuCo}_2\text{O}_4/\text{N-CNTs}/\text{P-GO}$ , and (c) GCE/ $\text{CuCo}_2\text{O}_4/\text{N-CNTs}/\text{P-GO}/\text{CUR}$ -imprinted poly (L-Cys); (C) Cyclic voltammograms of  $\text{K}_3\text{Fe}(\text{CN})_6$  ( $1 \text{ mmol L}^{-1}$ ) at scan rate of  $50 \text{ mV s}^{-1}$  obtained by: (a) GCE/ $\text{CuCo}_2\text{O}_4/\text{N-CNTs}/\text{P-GO}/\text{CUR}$ -imprinted poly (L-Cys), (b) GCE/ $\text{CuCo}_2\text{O}_4/\text{N-CNTs}/\text{P-GO}$ , (c) GCE/ $\text{CuCo}_2\text{O}_4/\text{N-CNTs}/\text{P-GO}/\text{CUR}$ -incorporated poly (L-Cys), (d) GCE. (A-C) condition: Start and stop potential: -0.6, Upper potential: 0.6, CUR to L-Cys mole ratio: 1:2, Electrolyte: KCl  $100 \text{ mmol L}^{-1}$ ; (D) Nyquist plots obtained from  $1 \text{ mmol L}^{-1}$   $\text{K}_3\text{Fe}(\text{CN})_6$  (solvated in KCl  $100 \text{ mmol L}^{-1}$ ) in the frequency range of  $10^2$  to  $10^5$  Hz by: (a) GCE/ $\text{CuCo}_2\text{O}_4/\text{N-CNTs}/\text{P-GO}/\text{CUR}$ -imprinted poly (L-Cys), (b) GCE/ $\text{CuCo}_2\text{O}_4/\text{N-CNTs}/\text{P-GO}$ , (c) GCE.

related to the O—H stretching ( $3367\text{ cm}^{-1}$ ), O—H bending ( $563\text{ cm}^{-1}$ ), C—O stretching ( $1393\text{ cm}^{-1}$ ,  $1125\text{ cm}^{-1}$ ), and C=O ( $1650\text{ cm}^{-1}$ ). Moreover the peaks appeared at  $2400\text{ cm}^{-1}$  (carbonitrile groups; RC≡N),  $1415\text{ cm}^{-1}$  (C=N in pyridinic groups),  $1640\text{ cm}^{-1}$  (C=C in CNTs),  $1564\text{ cm}^{-1}$  (C—N groups) and  $653\text{ cm}^{-1}$  (Co—O in  $\text{CuCo}_2\text{O}_4$ ) assigned to successful synthesis of  $\text{CuCo}_2\text{O}_4/\text{N-CNTs}$ . The P-GO FT-IR spectrum (Fig. 2A, curve b) shows stretching peaks of C—P, P=O, P—O, and P—OH at  $1128\text{ cm}^{-1}$ ,  $1167\text{ cm}^{-1}$ ,  $1058\text{ cm}^{-1}$ , and  $932\text{ cm}^{-1}$  respectively. Moreover, stretching peaks of P—H, C=C, C=O are centered at  $2406\text{ cm}^{-1}$ ,  $16046\text{ cm}^{-1}$ ,  $1723\text{ cm}^{-1}$ . The overlapping and broadening of stretching peak of OH with  $\text{CH}_2$  at  $2917\text{ cm}^{-1}$  and  $2846\text{ cm}^{-1}$  demonstrating the formation of phosphonic acid groups and less containing of carboxylic acid on GO (Etesami, Abouzari-Lotf, Ripin, Nasef, Ting, Saharkhiz, et al., 2018).

The successful formation of poly (L-Cys) on the surface of  $\text{CuCo}_2\text{O}_4/\text{N-CNTs}/\text{P-GO}$  was checked by FT-IR spectroscopy. As shown in the Fig. 2A, curve e the absorption peaks are appeared at  $3438\text{ cm}^{-1}$  is related to N—H stretching which is sharpened due to overlapping with O—H stretching band of  $\text{CuCo}_2\text{O}_4/\text{N-CNTs}$  at  $3367\text{ cm}^{-1}$ . It worth to mention that electrochemical oxidation of L-Cys on the surface lead to creation of cysteic acid which can be confirmed by appearance of absorption bands at  $1631\text{ cm}^{-1}$  as the combinational peak of stretching vibrations of C=O and C=C, and  $1064\text{ cm}^{-1}$  as stretching vibrations of C—N. Moreover absence of stretching vibration of S—H group of L-Cys at  $2550\text{ cm}^{-1}$  (Fig. 2A, curve d) in comparison with poly (L-Cys) (Fig. 2A, curve e) proved oxidization of S—H to  $\text{SO}_3\text{H}$  (Si, Jiang, Wang, Ding, & Luo, 2015). As presented in Fig. 2B, curve c (and Fig. 2A, curve c) the main vibration absorption bands of CUR are at  $810\text{ cm}^{-1}$  (=C—H),  $963\text{ cm}^{-1}$  (aliphatic C—O),  $1281\text{ cm}^{-1}$  (aromatic C—O),  $1510\text{ cm}^{-1}$  (C=C),  $1627\text{ cm}^{-1}$  (C=O), and O—H ( $3341\text{ cm}^{-1}$ ), which considerably covered by poly (L-Cys) (Fig. 2A, curve e, and Fig. 2B, curve b) which is in accordance with absorption bands presented in literature (Mars, Mejri, Hamzaoui, & Elfil, 2021). Also, as shown in Fig. 2B the FT-IR bands of poly (L-Cys)-CUR (Fig. 2B, curve b) possess stronger intensity and shift in comparison with poly (L-Cys) after removal of CUR (Fig. 2B, curve a), which obviously demonstrates that successful extraction procedure.

The further analysis of electrode morphology and topography was performed by AFM. According to the AFM images (Fig. 2C), nanoparticles uniformly covered electrode surface. As shown in Fig. 2C (part b) after formation of polymeric layer of poly (L-Cys)-CUR, the particles size increased in comparison with nanoparticles (Fig. 2C, part a). After removal of CUR from the polymeric layer, larger cavities (Fig. 2C, part c) were presented between particles demonstrating the successful formation of CUR-imprinted poly (L-Cys) on the electrode surface. Also, the root-mean-square (RMS) values, which used for expression of the surface roughness, obviously increased from  $3.78$  for nanoparticles to  $5.56\text{ nm}$  for poly (L-Cys)-CUR demonstrating successful formation of polymeric layer. Also, RMS value increased to  $29.47\text{ nm}$  for CUR-imprinted poly (L-Cys), which can be due to successful removal of CUR from poly (L-Cys) layer.

### 3.2. Cyclic voltammetry studies

In order to evaluation of effect of modifiers on the surface of the electrode, cyclic voltammograms were scanned in a solution of  $1\text{ mmol L}^{-1}\text{ K}_3[\text{Fe}(\text{CN})_6]$  and  $0.1\text{ mol L}^{-1}\text{ KCl}$  to estimate the active surface area of electrodes using Randles-Sevcik equation (Eq. (1)) as follow (Motia, Bouchikhi, & El Bari, 2021):

$$I_p = 2.69 \times 10^5 n^3/2 AD_0^{1/2} C_0 \nu^{1/2} \quad (1)$$

where  $I_p$ ,  $n$ ,  $A$ ,  $D_0$ ,  $n$  and  $C_0$  and  $\nu$  are related to the anodic peak current (amps), the number of electrons, the surface area of the electrode ( $\text{cm}^2$ ), the diffusion coefficient ( $\text{cm}^2\text{ s}^{-1}$ ), the number of electrons, the concentration ( $\text{mol cm}^{-3}$ ) of  $\text{K}_3[\text{Fe}(\text{CN})_6]$  in bulk solution and the scan rate

( $\text{V s}^{-1}$ ), respectively. For redox aforementioned system ( $\text{Fe}(\text{CN})_6^{3-/4-}$ )  $n$  and  $D_0$  values are  $1$  and  $7.6 \times 10^{-6}\text{ cm}^2\text{ s}^{-1}$ , respectively (Motia, Bouchikhi, & El Bari, 2021). Randles-Sevcik equation is related to an electrochemical reaction depended to the electrode potential and diffusion (Zaib & Athar, 2015). According to the Fig. 3A, by increasing scan rate, the cathodic and anodic peaks gradually increased and also there are a good relationship (Fig. 3B) between peak currents and square root of scan rate demonstrating diffusion controlled by mass transport (Wang, Chen, Li, Zhou, Guo, Kang, et al., 2018). The process of electron transfer can be mass transport if the process is wholly diffusion (Zaib & Athar, 2015). For calculation of surface area changes, the cyclic voltammograms of GCE (Fig. 3A, part a), GCE/ $\text{CuCo}_2\text{O}_4/\text{N-CNTs}/\text{P-GO}$  (Fig. 3A, part b) and GCE/ $\text{CuCo}_2\text{O}_4/\text{N-CNTs}/\text{P-GO}/\text{CUR-imprinted poly (L-Cys)}$  (Fig. 3A, part c) in a solution of  $1\text{ mmol L}^{-1}\text{ K}_3[\text{Fe}(\text{CN})_6]$  were scanned by increasing of scan rate from  $10\text{ mV s}^{-1}$  to  $100\text{ mV s}^{-1}$ . Using results of Fig. 3A, the alterations of anodic peak current (peak height;  $I_p$ ) versus  $\nu^{1/2}$  were plotted (Fig. 3B), and active surface area of GCE, GCE/ $\text{CuCo}_2\text{O}_4/\text{N-CNTs}/\text{P-GO}$  and GCE/ $\text{CuCo}_2\text{O}_4/\text{N-CNTs}/\text{P-GO}/\text{CUR-imprinted poly (L-Cys)}$  were calculated  $0.135\text{ cm}^2$ ,  $0.27\text{ cm}^2$  and  $0.54\text{ cm}^2$ , respectively, according to the Eq. (1). These indicates the improvement of surface area about 2 times with comparison of GCE and GCE/ $\text{CuCo}_2\text{O}_4/\text{N-CNTs}/\text{P-GO}$ , and 2 times with comparison of GCE/ $\text{CuCo}_2\text{O}_4/\text{N-CNTs}/\text{P-GO}$  and GCE/ $\text{CuCo}_2\text{O}_4/\text{N-CNTs}/\text{P-GO}/\text{CUR-imprinted poly (L-Cys)}$ . These phenomena proved effect of nanocomposite and creation of cavities on modification of electrode.

As shown in Fig. 3(C) redox peak current of GCE/ $\text{CuCo}_2\text{O}_4/\text{N-CNTs}/\text{P-GO}$  (Fig. 3C, curve b) was enhanced compared with GCE (Fig. 3C, curve d) due to high electron transfer capability of nanocomposite. According to the literature,  $\text{CuCo}_2\text{O}_4$  and N-CNTs are synergically able to enhancement conductivity and electrocatalytic activities due to increase of catalytic sites of Cu doping such as  $\text{Cu}^{2+}$  and Cu—N on the high specific surface area of CNTs which served as substrate for  $\text{CuCo}_2\text{O}_4$  (Cheng, Li, Su, Li, & Liu, 2017). Also, due to the electron-donor ability of P-doping and increase of conducting electrons density at Fermi level of carbon, the potential of electron transferring and conductivity of P-GO can be improved (X. Ma, Ning, Qi, Xu, & Gao, 2014).

The formation of poly (L-Cys)-CUR on the surface of GCE/ $\text{CuCo}_2\text{O}_4/\text{N-CNTs}/\text{P-GO}$ , led to somewhat decrease of redox peak current (peak height) due to the electron transfer hindrance (Fig. 3C, curve c). After elution of CUR molecules from poly (L-Cys), the current response (Fig. 3C, curve a) was considerably increased due to elimination of electron transfer hindrance of CUR molecules and creation of CUR-imprinted cavities leading to the enhancement of rate of electron transfer. According to the Fig. 3(C) peak potential separation ( $\Delta E_p$ ) of GCE/ $\text{CuCo}_2\text{O}_4/\text{N-CNTs}/\text{P-GO}$  was  $0.17\text{ V}$  which was significantly lower than  $\Delta E_p$  ( $0.27\text{ V}$ ) of GCE demonstrating catalytic effect of the nanocomposite. Moreover, formation of CUR-imprinted poly (L-Cys) on the surface of GCE/ $\text{CuCo}_2\text{O}_4/\text{N-CNTs}/\text{P-GO}$  decreased  $\Delta E_p$  ( $0.105\text{ V}$ ) due to poly (L-Cys) conductivity and formation of a lot of cavities which facilitate electron transfer.

### 3.3. EIS analysis

The resistance of electrode in different steps of modification can be performed by EIS using Nyquist impedance spectrum containing the semicircular section at higher frequencies and the linear section at lower frequencies (Kor & Zarei, 2016). The later indicates the diffusion-limiting process and the former is related to electron transfer resistance ( $R_{ct}$ ). In accordance with resulted Nyquist diagram, the possible circuit (Fig. 3D, inset) contained members including solution resistance ( $R_s$ ), double layer capacitance ( $C_{dl}$ ),  $R_{ct}$ , and Warburg impedance ( $Z_w$ ) which was in series with  $R_{ct}$  and is related to the Nernstian diffusion. According to the fitted circuit,  $R_{ct}$  is the only key element which describe the electrode kinetics for charge transfer (Kor & Zarei, 2016). According to the Nyquist impedance spectrum (Fig. 3D) which was obtained in  $1\text{ mmol L}^{-1}\text{ K}_3\text{Fe}(\text{CN})_6$  solution,  $R_{ct}$  value of GCE/ $\text{CuCo}_2\text{O}_4/\text{N-CNTs}/\text{P-GO}$

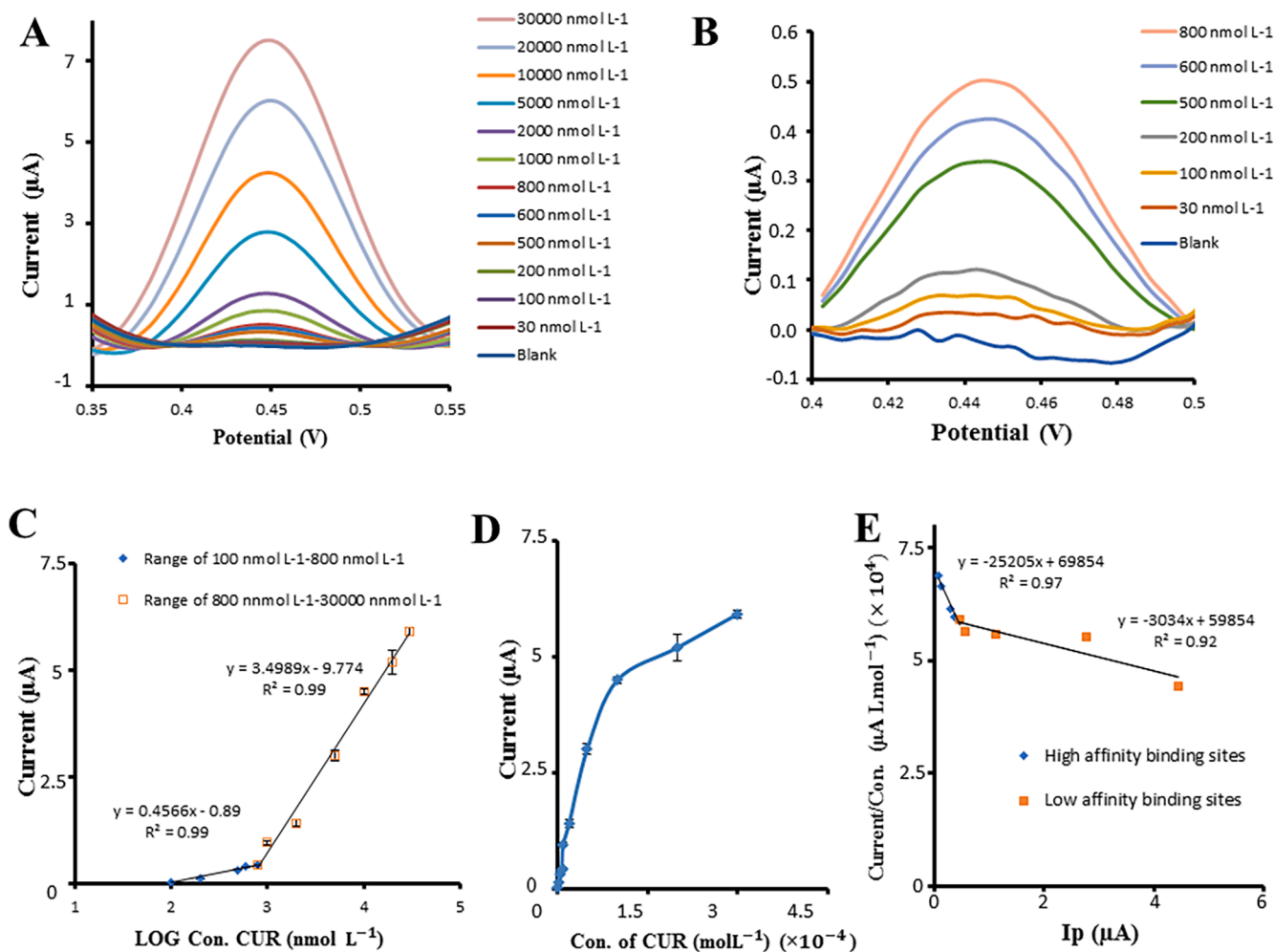


Fig. 4. (A, B) DPV peaks of CUR in the range of: (A) 30 nmol L<sup>-1</sup>–30000 nmol L<sup>-1</sup>, (B) 30 nmol L<sup>-1</sup>–800 nmol L<sup>-1</sup>; (C) Calibration curve for detection of CUR; (D) Binding isotherm of CUR on the modified sensor in the range of 100–30000 nmol L<sup>-1</sup>; (E) Schatchard plot which was plotted in two ranges of 100 nmol L<sup>-1</sup>–800 nmol L<sup>-1</sup> and 800 nmol L<sup>-1</sup>–30000 nmol L<sup>-1</sup>. Conditions: CUR to L-Cys mole ratio: 1:2, Electrolyte: PBS (pH 3.06, 0.1 mol L<sup>-1</sup>), Scan rate: 50 mV S<sup>-1</sup>.

(249 Ω) (Fig. 3D, curve b) is lower than GCE (339 Ω) (Fig. 3D, curve c). This phenomenon can be due to high conductivity and surface to volume ratio of nanocomposition which led to increasing rate of electron transfer. Fig. 3D indicates formation of MIP considerably reduced  $R_{ct}$  to 4 Ω (Fig. 3D, curve a) and the reduce of semicircle radius demonstrating successful removal of CUR from poly (L-Cys) matrix and formation of numerous cavities which promotes electron transfer pathways.

### 3.4. Determination of CUR

In order to quantification of CUR, DPV mode with was used due to advantages of peak sharpening, great sensitivity and low background. As shown in Scheme 1 after electropolymerization of L-Cys on the GCE/CuCo<sub>2</sub>O<sub>4</sub>/N-CNTs/P-GO by consecutive nucleophilic acyl substitution (He, Li, Zhang, & Luo, 2017), CUR trapped in poly (L-Cys) matrix through hydrogen bonding interactions. After removal of CUR, numerous selective cavities which were complementary in functional groups and shape with CUR were created. After rebinding of CUR, one electron oxidation process led to creation of DPV peak (Q. Zhou, Zhai, Pan, & Li, 2017). As shown in Fig. 4A and Fig. 4B oxidation peaks of CUR were increased by increase of CUR in range of 0.1–30 μmol L<sup>-1</sup>. The calibration curve (Fig. 4C) which plotted by variations of peak current versus CUR concentrations demonstrates two linear ranges of 0.1–0.8 μmol L<sup>-1</sup> ( $y = 0.4566x - 0.89$ ,  $R^2 = 0.99$ ) and 0.8–30 μmol L<sup>-1</sup> ( $y = 3.4989x - 9.774$ ,  $R^2 = 0.99$ ) with limit of detection (LOD) of 30 nmol L<sup>-1</sup>.

The resulted data of proposed sensor for detection of CUR was compared with previous studies. The summarized data of Table 1 obviously demonstrated that linear range and LOD of present study was acceptable in comparison with other studies and proposed sensor was successfully designed for detection of CUR. According to the information was reported in Table 1, although some chromatography-based studies possess better linear range or LOD, but these methods are highly depended on the complex and expensive equipment and highly experienced experts in comparison with electrochemical sensors. Moreover, other reported sensors for CUR have not been designed based on incorporation of nanoparticles with MIP which can donate sensitivity and selectivity to designed sensor.

Due to validation of method, different parameter such as repeatability, precision, bias and accuracy of proposed method for intra-day (n = 4) and inter-day (n = 4) detection of CUR were evaluated according to the previous study (Kalambate, Rawool, & Srivastava, 2016). Moreover, the recovery was estimated using calibration curve. According to the results of Table 2, acceptable precision and accuracy of proposed method for detection of CUR were confirmed.

### 3.5. Binding studies

In order to demonstration of imprinted polymers superiority, evaluation of binding constants is necessary. Due to the presence of numerous heterogeneous binding sites in non-covalently MIP,

**Table 1**

Summarized data of CUR detection methods.

Sensor/Extraction method	Detection	Linear range	LOD	Sample	Recovery	Reference
Degradation product	HPLC	203.59–475.05 $\mu\text{mol L}^{-1}$ (0.075–0.175 mg $\text{mL}^{-1}$ )	38 $\mu\text{mol L}^{-1}$ (0.014 mg $\text{mL}^{-1}$ )	dosage forms (tablets and capsules)	100.35–101.21	(Korany, Haggag, Ragab, & Elmallah, 2017)
chloroform and ethyl acetate extraction	HPLC	0.013–0.067 $\mu\text{mol L}^{-1}$ (5–25 ngmL <sup>-1</sup> ) and 0.067–0.68 $\mu\text{mol L}^{-1}$ (25–250 ngmL <sup>-1</sup> )	0.0067 $\mu\text{mol L}^{-1}$	plasma	66–78	(Pak, Patek, & Mayersohn, 2003)
Extraction with ethyl acetate/methanol organic solvents	HPLC	0.543–19 $\mu\text{mol L}^{-1}$ (0.2–7.0 $\mu\text{g}$ $\text{mL}^{-1}$ )	0.247 $\text{nmol L}^{-1}$ (0.091 $\text{ng mL}^{-1}$ )	plasma and urine	>96	(Heath, Pruitt, Brenner, & Rock, 2003)
methanol precipitation	LC-MS/MS	13.57–5429.17 $\text{nmol L}^{-1}$ (5–2000 $\text{ng mL}^{-1}$ )	13.57 $\text{nmol L}^{-1}$ (5 $\text{ng mL}^{-1}$ )	rat plasma	98–106	(W. Ma, Wang, Guo, & Tu, 2015)
solid-phase extraction (SPE) cartridge based on the material of tributyl phosphate resin	Capillary electrophoresis with amperometric detection (CE-AD)	3–700 $\mu\text{mol L}^{-1}$	30 $\text{nmol L}^{-1}$	extracts of turmeric	81.0–85.5	(Sun, Gao, Cao, Yang, & Wang, 2002)
nickel chloride solution modified (NiCl <sub>2</sub> )- modified GCE	Electrochemical (DPV)	10–600 $\mu\text{mol L}^{-1}$	0.109 $\mu\text{mol L}^{-1}$	human blood serum	99.9–100.3	(Zokhtareh & Rahimnejad, 2018)
MIP-modified carbon paste electrode (MIP-CPE)	Electrochemical (CV)	0.1–50 $\mu\text{mol L}^{-1}$	10.1 $\text{nmol L}^{-1}$	curcuma powder and cookies	90.77–105.7	(Q. Zhou, Zhai, Pan, & Li, 2017)
GCE	Electrochemical (CV)	9.9–107 $\mu\text{mol L}^{-1}$	4.1 $\mu\text{mol L}^{-1}$	spices	99–100	(Ziyatdinova, Nizamova, & Budnikov, 2012)
Al <sup>3+</sup> ions on palladium nanoparticles (PdNps)-coated graphite electrode (Al <sup>3+</sup> /PdNp/GE)	Electrochemical (SWV)	0.03–0.6 $\mu\text{mol L}^{-1}$	22 $\text{nmol L}^{-1}$	marketed spices sample of turmeric powder	–	(Çakır, Biçer, & Arslan, 2015)
nitrogen and phosphorus dual-doped carbon dots (NP-Cdots)	Fluorescence quenching	0.5–20 $\mu\text{mol L}^{-1}$	58 $\text{nmol L}^{-1}$	drinking water and the food samples	95.2–105.2	(Liu, Gong, Dong, Zhou, Shuang, & Dong, 2018)
GCE/CuCo <sub>2</sub> O <sub>4</sub> /N-CNTs/P-GO/CUR- imprinted poly (L-Cys)	Electrochemical (DPV)	0.1–30 $\mu\text{mol L}^{-1}$	30 $\text{nmol L}^{-1}$	Serum	80–110.87	Present study

**Table 2**

Evaluation of repeatability, precision and bias by proposed method for detection of CUR.

Detection	Added ( $\mu\text{mol L}^{-1}$ )	Found ( $\mu\text{mol L}^{-1}$ )	Recovery (%)	Bias (%)	RSD (%)
Intra-day (n = 4)	0.350	0.346	98.90	1.095	3.04
Inter-day (n = 4)	6	5.75	95.94	4.058	5.09

proficiency of MIP for analytical procedure may be decreased and led to the cross-reactivity during binding assay (Schauperl & Lewis, 2015). So, recognition and estimation of the heterogeneity and different sites can be importance. For this purpose, the binding isotherms is determined using detection responses related to a range of concentration. Subsequently a suitable model is fit to the binding isotherm to evaluate the binding parameters. The Langmuir isotherm is a prevalent model which have been used (Pesavento, Marchetti, De Maria, Zeni, & Cennamo, 2019).

According to the previous study (Pesavento, Marchetti, De Maria, Zeni, & Cennamo, 2019), binding evaluation of synthesized polymeric layer was performed using following equation (Eq. (2)) related to Langmuir model:

$$S = \frac{k_{CR}K_A[A]}{1 + K_A[A]} \quad (2)$$

The linearized form of Eq. (2) is as follow:

$$\frac{S}{[A]} = K_A S + K_A k_{CR} \quad (3)$$

The parameters of Eq. (2) and Eq. (3) such as S, [A], K<sub>A</sub>, k, and C<sub>R</sub> are known as signal, target concentration (mol L<sup>-1</sup>), association constant (L mol<sup>-1</sup>), transduction method constant, and sites concentration, respectively. As shown in Fig. 4D, the binding isotherm plot was curved at high concentrations due to saturation which is in accordance with Langmuir model. Moreover, curved Scatchard plot (Fig. 4E) indicated two straight lines related to the presence of two different kinds of sites with high and low affinity, due to the complete and incomplete interaction between CUR and poly (L-Cys) (Mohammadinejad, Kamrani Rad, Karimi, Motamedshariaty, & Mohajeri, 2021). Also, according to the Eq. (3), values of K<sub>A</sub> for high and low affinity binding sites were calculated 2.52 × 10<sup>4</sup> L mol<sup>-1</sup> and 3.03 × 10<sup>3</sup> L mol<sup>-1</sup>, respectively. The selectivity and specificity of prepared imprinted polymer can be evaluated by K<sub>A</sub> (Hasanah, Rahayu, Pratiwi, Rostinawati, Megantara, Saputri, et al., 2019). The estimated values of K<sub>A</sub> were in acceptable range in comparison with K<sub>A</sub> values reported by previous studies which introduced MIP-based sensors for ethyl carbamate (K<sub>A</sub> 4.75 × 10<sup>6</sup> L mol<sup>-1</sup> (Guo, Hu, Wang, Brodelius, & Sun, 2018)) erythromycin (K<sub>A</sub> 6.25 × 10<sup>5</sup> L mol<sup>-1</sup> (Sari, Üzek, Duman, & Denizli, 2016)), dopamine (K<sub>A</sub> 2.9 × 10<sup>4</sup> L mol<sup>-1</sup> (Li, Zhang, Sun, Bai, & Zheng, 2016)), methyl parathion (K<sub>A</sub> 0.029 L mg<sup>-1</sup>; 7.63 × 10<sup>3</sup> L mol<sup>-1</sup> (Hassan, Moura, Ali, Moselhy, Sotomayor, & Pividori, 2018)), azithromycin (K<sub>A</sub> 3.5 × 10<sup>3</sup> L mol<sup>-1</sup> (Stoian, Iacob, Dudaş, Barbu-Tudoran, Bogdan, Marian, et al., 2020)), fructose (K<sub>A</sub> 4.1 × 10<sup>2</sup> L mol<sup>-1</sup> (Nikitina, Zaryanov, Kochetkov, Karyakina, Yatsimirsky, & Karyakin, 2017)), lactate (K<sub>A</sub> 1.50 × 10<sup>2</sup> L mol<sup>-1</sup> (Nikitina, Zaryanov, Kochetkov, Karyakina, Yatsimirsky, & Karyakin, 2017)), and glucose

**Table 3**

Results of CUR detection in serum sample.

Sample	Added (nmol L <sup>-1</sup> )	Found (nmol L <sup>-1</sup> )	Recovery (%)	RSD (%; n = 3)
1	600	614	102.33	0.87
2	800	887	110.87	0.76
3	1000	1060	106.00	4.89
4	2000	2010	100.20	0.53
5	5000	4000	80.00	5.81
6	7000	6730	96.14	5.78
7	10,000	9630	96.30	1.64

(K<sub>A</sub> 35 L mol<sup>-1</sup> (Nikitina, Zaryanov, Kochetkov, Karyakina, Yatsimirsky, & Karyakin, 2017)).

### 3.6. Real sample

In order to evaluation of the feasibility of proposed sensor, the serum sample spiked with various concentration of CUR and analyzed by DPV method. As shown in the Table 3 the recovery values are ranged from 80 to 110.87 % which confirmed the low interferences from the matrix can be happened for detection of CUR. Moreover, according to the data of Table 3, repeatability (RSD%) for triplicate detection of CUR in serum sample was in the range of 0.76–5.81 %. The real sample study obviously proved that introduced sensor is highly efficient and applicable for accurate and precise detection of CUR in different real samples such as biological samples.

## 4. Conclusion

Herein, an electrochemical sensor was designed through modification of GCE by CuCo<sub>2</sub>O<sub>4</sub>/N-CNTs/P-GO nanocomposite which followed by electrochemical covering the modified electrode surface by poly (L-Cys) layer in presence of CUR. In the next step, removal of CUR from poly (L-Cys) matrix created cavities with high affinity toward CUR according to the shape and functional groups. As far as we know it was for the first time that aforementioned design was used for detection of CUR. The CV and EIS studies obviously demonstrated that catalytic and conductivity features potentially increased after dropping the CuCo<sub>2</sub>O<sub>4</sub>/N-CNTs/P-GO nanocomposite and formation of CUR-imprinted poly (L-Cys) on the electrode surface. These phenomena were happened due to the synergic features such as catalytic activity of Cu-doping sites, high specific surface area of CNTs, electron-donor ability of P-doping sites, high conducting electrons density at Fermi level of carbons of GO, and electron transfer facilitation of numerous specific cavities. The designed sensor was successfully used for detection of CUR in the wide linear ranges of 0.1–0.8 μmol L<sup>-1</sup> and 0.8–30 μmol L<sup>-1</sup>, and acceptable LOD of 30 nmol L<sup>-1</sup>. Moreover, the as-constructed electrochemical sensor was successfully used for detection of CUR in serum sample with favorable recoveries (80–110.87%). The obtained results proved that this simple and fast response method can be powerfully used for detection and monitoring CUR in biological samples.

### CRedit authorship contribution statement

**Arash Mohammadnejad:** Formal analysis, Methodology, Software, Validation, Investigation, Writing – original draft, Writing – review & editing, Visualization. **Ebrahim Abouzari-Lotf:** Investigation, Resources. **Ghazaleh Aleyaghoob:** Formal analysis, Investigation. **Majid Rezayi:** Conceptualization, Resources, Supervision. **Reza Kazemi Oskuee:** Resources, Project administration, Funding acquisition.

### Declaration of Competing Interest

The authors declare that they have no known competing financial interests or personal relationships that could have appeared to influence

the work reported in this paper.

### Acknowledgement

The authors gratefully acknowledge the Vice Chancellor of Research of Mashhad niversity of Medical Sciences, Mashhad, Iran.

### Funding

This study supported by Vice Chancellor of Research of Mashhad niversity of Medical Sciences, Mashhad, Iran, through the grant number 981484.

## References

- Abouzari-Lotf, E., Zakeri, M., Nasef, M. M., Miyake, M., Mozarmnia, P., Bazilah, N. A., ... Ahmad, A. (2019). Highly durable polybenzimidazole composite membranes with phosphonated graphene oxide for high temperature polymer electrolyte membrane fuel cells. *Journal of Power Sources*, 412, 238–245.
- Çakır, S., Biçer, E., & Arslan, E. Y. (2015). A newly developed electrocatalytic oxidation and voltammetric determination of curcumin at the surface of PdNp-graphite electrode by an aqueous solution process with Al<sup>3+</sup>. *Croatica Chemica Acta*, 88(2), 105–112.
- Cheng, H., Li, M. L., Su, C. Y., Li, N., & Liu, Z. Q. (2017). Cu□ Co Bimetallic Oxide Quantum Dot Decorated Nitrogen-Doped Carbon Nanotubes: A High-Efficiency Bifunctional Oxygen Electrode for Zn–Air Batteries. *Advanced Functional Materials*, 27(30), 1701833.
- Etesami, M., Abouzari-Lotf, E., Ripin, A., Nasef, M. M., Ting, T. M., Saharkhiz, A., & Ahmad, A. (2018). Phosphonated graphene oxide with high electrocatalytic performance for vanadium redox flow battery. *International Journal of Hydrogen Energy*, 43(1), 189–197.
- Guo, M., Hu, Y., Wang, L., Brodelius, P. E., & Sun, L. (2018). A facile synthesis of molecularly imprinted polymers and their properties as electrochemical sensors for ethyl carbamate analysis. *RSC Advances*, 8(69), 39721–39730.
- Hasanah, A. N., Rahayu, D., Pratiwi, R., Rostinawati, T., Megantara, S., Saputri, F. A., & Puspanegara, K. H. (2019). Extraction of atenolol from spiked blood serum using a molecularly imprinted polymer sorbent obtained by precipitation polymerization. *Heliyon*, 5(4), Article e01533.
- Hassan, A. H., Moura, S. L., Ali, F. H., Moselhy, W. A., Sotomayor, M. d. P. T., & Pividori, M. I. (2018). Electrochemical sensing of methyl parathion on magnetic molecularly imprinted polymer. *Biosensors and Bioelectronics*, 118, 181–187.
- He, D., Li, S., Zhang, P., & Luo, H. (2017). CVD graphene incorporating polymerized l-cysteine as an electrochemical sensing platform for simultaneous determination of dopamine and ascorbic acid. *Analytical Methods*, 9(47), 6689–6697.
- Heath, D. D., Pruitt, M. A., Brenner, D. E., & Rock, C. L. (2003). Curcumin in plasma and urine: Quantitation by high-performance liquid chromatography. *Journal of Chromatography B*, 783(1), 287–295.
- Kalambate, P. K., Rawool, C. R., & Srivastava, A. K. (2016). Voltammetric determination of pyrazinamide at graphene-zinc oxide nanocomposite modified carbon paste electrode employing differential pulse voltammetry. *Sensors and Actuators B: Chemical*, 237, 196–205.
- Kor, K., & Zarei, K. (2016). Development and characterization of an electrochemical sensor for furosemide detection based on electropolymerized molecularly imprinted polymer. *Talanta*, 146, 181–187.
- Korany, M. A., Haggag, R. S., Ragab, M. A., & Elmallah, O. A. (2017). A validated stability-indicating HPLC method for simultaneous determination of Silymarin and Curcumin in various dosage forms. *Arabian Journal of Chemistry*, 10, S1711–S1725.
- Li, J., Zhang, N., Sun, Q., Bai, Z., & Zheng, J. (2016). Electrochemical sensor for dopamine based on imprinted silica matrix-poly (aniline boronic acid) hybrid as recognition element. *Talanta*, 159, 379–386.
- Liang, P., Wang, F., & Hu, Z.-A. (2018). Controlled synthesis of ordered sandwich CuCo<sub>2</sub>O<sub>4</sub>/reduced graphene oxide composites via layer-by-layer heteroassembly for high-performance supercapacitors. *Chemical Engineering Journal*, 350, 627–636.
- Liang, Z.-H., Zhu, Y.-J., & Hu, X.-L. (2004). β-Nickel hydroxide nanosheets and their thermal decomposition to nickel oxide nanosheets. *The Journal of Physical Chemistry B*, 108(11), 3488–3491.
- Liu, Y., Gong, X., Dong, W., Zhou, R., Shuang, S., & Dong, C. (2018). Nitrogen and phosphorus dual-doped carbon dots as a label-free sensor for Curcumin determination in real sample and cellular imaging. *Talanta*, 183, 61–69.
- Ma, W., Wang, J., Guo, Q., & Tu, P. (2015). Simultaneous determination of doxorubicin and curcumin in rat plasma by LC-MS/MS and its application to pharmacokinetic study. *Journal of Pharmaceutical and Biomedical Analysis*, 111, 215–221.
- Ma, X., Ning, G., Qi, C., Xu, C., & Gao, J. (2014). Phosphorus and nitrogen dual-doped few-layered porous graphene: A high-performance anode material for lithium-ion batteries. *ACS Applied Materials & Interfaces*, 6(16), 14415–14422.
- Mars, A., Mejri, A., Hamzaoui, A. H., & Elfil, H. (2021). Molecularly imprinted curcumin nanoparticles decorated paper for electrochemical and fluorescence dual-mode sensing of bisphenol A. *Microchimica Acta*, 188(3), 1–11.

- Mohammadinejad, A., Kamrani Rad, S. Z., Karimi, G., Motamedshariaty, V. S., & Mohajeri, S. A. (2021). Preparation, evaluation, and application of dummy molecularly imprinted polymer for analysis of hesperidin in lime juice. *Journal of Separation Science*, *44*(7), 1490–1500.
- Motia, S., Bouchikhi, B., & El Bari, N. (2021). An electrochemical sensor based on molecularly imprinted polymer conjointly with a voltammetric electronic tongue for quantitative diphenyl phosphate detection in urine samples from cosmetic product users. *Sensors and Actuators B: Chemical*, *332*, Article 129449.
- Mousaabadi, K. Z., Ensafi, A. A., Hadadzadeh, H., & Rezaei, B. (2020). Reduced graphene oxide and carbon nanotubes composite functionalized by azobenzene, characterization and its potential as a curcumin electrochemical sensor. *Journal of Electroanalytical Chemistry*, *873*, Article 114418.
- Neerati, P., Devde, R., & Gangi, A. K. (2014). Evaluation of the effect of curcumin capsules on glyburide therapy in patients with type-2 diabetes mellitus. *Phytotherapy Research*, *28*(12), 1796–1800.
- Nikitina, V. N., Zaryanov, N. V., Kochetkov, I. R., Karyakina, E. E., Yatsimirsky, A. K., & Karyakin, A. A. (2017). Molecular imprinting of boronate functionalized polyaniline for enzyme-free selective detection of saccharides and hydroxy acids. *Sensors and Actuators B: Chemical*, *246*, 428–433.
- Pak, Y., Patek, R., & Mayersohn, M. (2003). Sensitive and rapid isocratic liquid chromatography method for the quantitation of curcumin in plasma. *Journal of Chromatography B*, *796*(2), 339–346.
- Pesavento, M., Marchetti, S., De Maria, L., Zeni, L., & Cennamo, N. (2019). Sensing by molecularly imprinted polymer: Evaluation of the binding properties with different techniques. *Sensors*, *19*(6), 1344.
- Priyanga, S., Khamrang, T., Velusamy, M., Karthi, S., Ashokkumar, B., & Mayilmurugan, R. (2019). Coordination geometry-induced optical imaging of l-cysteine in cancer cells using imidazopyridine-based copper (ii) complexes. *Dalton Transactions*, *48*(4), 1489–1503.
- Sari, E., Üzek, R., Duman, M., & Denizli, A. (2016). Fabrication of surface plasmon resonance nanosensor for the selective determination of erythromycin via molecular imprinted nanoparticles. *Talanta*, *150*, 607–614.
- Schauperl, M., & Lewis, D. W. (2015). Probing the structural and binding mechanism heterogeneity of molecularly imprinted polymers. *The Journal of Physical Chemistry B*, *119*(2), 563–571.
- Si, X., Jiang, L., Wang, X., Ding, Y., & Luo, L. (2015). Determination of isoniazid content via cysteine acid/graphene modified glassy carbon electrode. *Analytical Methods*, *7*(2), 793–798.
- Stoian, I.-A., Iacob, B.-C., Dudaş, C.-L., Barbu-Tudoran, L., Bogdan, D., Marian, I. O., ... Oprean, R. (2020). Biomimetic electrochemical sensor for the highly selective detection of azithromycin in biological samples. *Biosensors and Bioelectronics*, *155*, Article 112098.
- Sun, X., Gao, C., Cao, W., Yang, X., & Wang, E. (2002). Capillary electrophoresis with amperometric detection of curcumin in Chinese herbal medicine pretreated by solid-phase extraction. *Journal of Chromatography A*, *962*(1–2), 117–125.
- Wang, H.-H., Chen, X.-J., Li, W.-T., Zhou, W.-H., Guo, X.-C., Kang, W.-Y., ... Tian, Q.-W. (2018). ZnO nanotubes supported molecularly imprinted polymers arrays as sensing materials for electrochemical detection of dopamine. *Talanta*, *176*, 573–581.
- Xu, H., Liu, J., Chen, Y., Li, C.-L., Tang, J., & Li, Q. (2017). Synthesis of three-dimensional nitrogen-doped graphene/polyaniline hydrogels for high performance supercapacitor applications. *Journal of Materials Science: Materials in Electronics*, *28*(14), 10674–10683.
- Zaib, M., & Athar, M. M. (2015). Electrochemical evaluation of phanerocheaete chrysochlorium based carbon paste electrode with potassium ferricyanide redox system. *International Journal of Electrochemical Science*, *10*(8), 6690–6702.
- Zhang, J., Sui, R., Xue, Y., Wang, X., Pei, J., Liang, X., & Zhuang, Z. (2019). Direct synthesis of parallel doped N-MoP/N-CNT as highly active hydrogen evolution reaction catalyst. *Science China Materials*, *62*(5), 690–698.
- Zhou, Q., Zhai, H., Pan, Y., & Li, K. (2017). A simple and sensitive sensor based on a molecularly imprinted polymer-modified carbon paste electrode for the determination of curcumin in foods. *RSC Advances*, *7*(37), 22913–22918.
- Zhou, W., Mo, F., Sun, Z., Luo, J., Fan, J., Zhu, H., ... Zhang, X. (2022). Bright red-emitting P, Br co-doped carbon dots as “OFF-ON” fluorescent probe for Cu<sup>2+</sup> and L-cysteine detection. *Journal of Alloys and Compounds*, *897*, Article 162731.
- Ziyatdinova, G., Nizamova, A., & Budnikov, H. (2012). Voltammetric determination of curcumin in spices. *Journal of Analytical Chemistry*, *67*(6), 591–594.
- Zokhtareh, R., & Rahimnejad, M. (2018). A novel sensitive electrochemical sensor based on nickel chloride solution modified glassy carbon electrode for curcumin determination. *Electroanalysis*, *30*(5), 921–927.